PAPER

Check for updates

Quantum dynamics of $C_{10}H^-$ in the interstellar medium: inelastic collisions with He and formation reaction from the $HC_{10}H/H^-$ reactants†

J. Alonso de la Fuente, [a] L. González-Sánchez, [b] E. Yurtsever, [c] C. Sanz-Sanz, [d] M. Satta, [e] R. Wester [f] and F. A. Gianturco [*f]

The anion $C_{10}H^-$ is the largest of the linear (C,H)-bearing chains detected so far in the Interstellar Medium. It is therefore important to investigate both possible chemical routes to its formation and the efficiency of it producing rotational excited states *via* collision with other abundant partners. Here we therefore present and discuss the general features of a new *ab initio* potential energy surface for the interaction of this linear anion with He and use it to generate its rotationally inelastic quantum collision rate coefficients. Additionally, we carry out a quantum study of the possible formation of the title anion coming from the H^- anion reacting with the $HC_{10}H$ neutral precursor, also detected in the same environments. We employ a Legendre Polynomials expansion representation for the purely inelastic interaction while for the reactive process we generate a reduced-dimensionality formulation and employ it within the variational transition state theory (VTST) approach including long-range (LR) corrections. We found that the final inelastic rate coefficients for this anion are all fairly large and that the suggested formation reaction also yields rate coefficients at the cloud's low temperatures which are large enough to be significant, hence to be included within existing chemical networks dealing with polyyne ions formations. The consequences of such findings for the anion's non-equilibrium populations in interstellar environments are discussed in our conclusions.

a Instituto de Física Fundamental, IFF-CSIC, C/Serrano 123, 28006 Madrid, Spain

b Departamento de Química Física, University of Salamanca Plaza de los Caídos sn, 37008, Salamanca, Spain

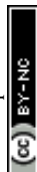*c Dept of Chemistry, Koç University, Rumelifeneriyolu, Sariyer, TR-34450, Istanbul, Turkey*

d Departamento de Quimica Fisica Aplicada, Modulo 14, Universidad Autonoma de Madrid, 28049 Madrid, Spain

e CNR-ISMN and Dept of Chemistry, The University of Rome Sapienza, P.le A. Moro 5, 00185 Rome, Italy

f Institut fuer Ionenphysik und Angewandte Physik, Universitaet Innsbruck, Technikerstr. 25, A-6020, Innsbruck, Austria.
E-mail: francesco.gianturco@uibk.ac.at

† The present study is dedicated to Professor N. N. Sathyamurthy, on the occasion of his 75th birthday. We wish him, a dear friend and an outstanding scientist, many years of happy research and collaborations with many colleagues around the world.

1 Introduction

It has now been nearly 20 years since the first reported molecular anion was detected in astronomical environments with the discovery of C_6H^-, a culmination of the early predictions that anions should be present under interstellar conditions.[1–4] The above studies made abundantly clear that molecular anions are critically important to the physics and evolution of astronomical species, including building up structures in the early universe, dominating the visible opacity for stars like the Sun. They are also considered today as being the possible carriers to the diffuse interstellar bands, and capable of determining the physical and chemical environments of astrophysical regions including the impact of interstellar radiation fields and other molecular cloud properties. Thus, the relatively recent discovery of negative ions in the interstellar medium has created over the years a great deal of interest and activity in the further search for their possible presence in different regions. Various molecular anions have been discovered to date in several different sources.[5,6] More specifically, eight anions were observed as having linear carbon chains of the form C_nN^- with $n = 1, 3, 5, 7$ and C_nH^- with $n = 4, 6, 8, 10$. They have mostly been identified in the circumstellar envelope IRC+10216 and in the dense regions of the Taurus molecular cloud known under the name TMC-1. Further variants of these anions have been suggested as present (but not yet confirmed), regarding additional systems like C_2H^- and C_9N^-. The issue of the possible relevance of negative ion formation has been discussed in the literature for the past thirty years or so.[1,2,4] The recent observation in an important Circumstellar Envelope (CSE) of the longest chain so far of an anionic polyyne, the $C_{10}H^-$, as well as the $HC_{10}H$ species,[7] has further spurred the search for more chemical explanations as to

This journal is © the Owner Societies 2025

*Phys. Chem. Chem. Phys.*, 2025, **27**, 21231–21243 | 21231

their formation routes. The simplest of all anions, the H^- ion, has in fact played a significant role in astrophysics for many decades and has been proposed since the 1930s as an important source of the continuum opacity of the Sun even before its structure had been fully understood. It has also been studied via a great variety of experimental and theoretical approaches.[8] Although it has yet to be detected outside the laboratory observation of its properties, it has been often surmised as an important partner in astrochemical processes,[8] so that H^- has been involved within possible chemical networks which are expected to actively proceed to the formation of molecular anions, either observed or stipulated to be present in the interstellar medium (ISM) (e.g., see ref. 9 for a recent study). An interesting formation route for H^- was put forward a while ago by ref. 10, whereby the gas phase radiative association was replaced by a process in which thermal H atoms attach an electron located on the surface of dust grains. This would then provide a more efficient route, producing H_2 more in line with what observations expect.[11] The actual abundance of this simple anion in the ISM, however, is still an open question which, besides being surmised as present by several network models, e.g., see ref. 12, could indeed support its importance within chemical networks that are leading to the formation of larger, more complex molecular anions.

In the present work, spurred by the recent observation of C-bearing chains like the neutral $HC_{10}H$ and the anionic $C_{10}H^-$,[7] we have decided to investigate from accurate quantum calculations two important features involving this anion: the collision interaction of the long chain with He atoms and the reaction involving the neutral radical with H^-. The latter reaction is found, as we shall discuss below, to efficiently produce the $C_{10}H^-$ anion in the same CSEs.[5,6] The computed rotational inelastic rates coefficient from collisions with He are also found to be of significant size, as further discussed below. In an earlier study of ours[36] we had analysed a simple modeling of the interaction of various anions, including the present chain, with H_2 to produce scaled estimates of the rate coefficients. Because of the approximate nature of that study, we shall further discuss it in our future work on the exact dynamics for calculating collision rate coefficients for the H_2 partner of the long-chain anions, while limiting our present results to exact interaction forces and quantum dynamics.

In order to be able to put more realistic limits to the abundances which can be obtained for the chemical processes within dense clouds, one should note that they have typical temperatures between about 10 K and 50 K, with a density varying between 100 cm^{-3} and 10^4 cm^{-3}, so that our quantum reactive analysis, as well as the rotational inelastic processes, will be chiefly discussed within that lower range of temperatures.

The energy-transfer collisions which we will be discussing in the present work, will be produced by the following quantum process:

$$He + HC_{10}^-(j_i) \rightarrow He + HC_{10}^-(j_i') \quad (1)$$
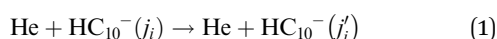
While for the formation reaction of the anion we shall be investigating the following reactive process:

$$H^- + HC_{10}H \rightarrow H_2 + HC_{10}^- \quad (2)$$
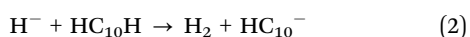
In some of our earlier studies,[13,14] similar reactions with other linear anions were treated as evolving via largely collinear processes between shorter chains of polyynes and the H^- partner.[13] We had found such reactions to be barrierless, without formation of long-lived transition states and strongly exothermic by about 3.0 to 5.0 eV. These features were found to also hold for longer chains, which again follow in the main a chiefly linear reaction path.[14]

The next Section 2 will discuss in detail the calculation of both the reactive potential energy surface (RPES) needed to study reaction (2) and the subreactive potential energy surface (PES) which will be responsible for driving rotational state-changing processes in collisions with He atoms as given by reaction (1). That same section will also describe some of the features obtained from the fitting of the inelastic interaction potential. The quantum reactive method employed for calculating the final reaction rate coefficient will be discussed in Section 3, while Section 4 will report all our results and Section 5 will present our conclusions.

2 Ab initio interactions in a multidimensional framework

2.1 Structures of anionic and radical chains

Calculations were carried out for the two molecular partners involved in reaction (2) (see later), i.e. for the $HC_{10}H$ reagent and the $C_{10}H^-$ product, using MOLPRO version 2010.1, see: ref. 15–17. The various C–C distances in the two molecules are very similar and they were both fully optimized using the MP2 method in MOLPRO and employing the cc-pVQZ basis set. All structures correspond to true minima and all the Hessian eigenvalues are positive. Table 1 presents the optimized values (all given in units of Å) of all the C–C ($r_i - r_j$) and the HC (H_b–C) bond distances for both the radical and the anion.

2.2 The reactive minimum energy path

Due to their usually large rate coefficients, barrierless reactions are of key importance in a variety of chemical situations, including the combustion, atmospheric, and interstellar environments. In the present case, as summarized in the Introduction, we have suggested that reaction (2) could be a possible path to forming the present anion because, as we shall further

Table 1 Computed optimized bond distances for the neutral radical, the anion and its neutral structure. All in units of Å

MP2/VQZ	$C_{10}H^-$	$HC_{10}H$	$C_{10}H$
H–C	1.0602	1.0620	1.0627
r_{1-2}	1.2270	1.2216	1.2203
r_{2-3}	1.3480	1.3524	1.3530
r_{3-4}	1.2444	1.2344	1.2308
r_{4-5}	1.3285	1.3404	1.3428
r_{5-6}	1.2532	1.2376	1.2325
r_{6-7}	1.3203	1.3404	1.3372
r_{7-8}	1.2555	1.2344	1.2413
r_{8-9}	1.3283	1.3524	1.3184
r_{9-10}	1.2727	1.2216	1.2917
H_b–C		1.0620	

21232 | Phys. Chem. Chem. Phys., 2025, **27**, 21231–21243

This journal is © the Owner Societies 2025

show below, such a reaction is indeed exothermic, without a long-lived pre-reactive complex, and follows a largely collinear configuration, as discussed in ref. 9 and 14.

In our previous studies we had also identified for such reactions the presence of two reasonably distinct 'complex-forming' regions within the quasi-linear coordinates involved in the process.[13] These two regions correlate with two different aspects of the RPES. The "outer" region correlates qualitatively with the location of the centrifugal barriers on the long-range part of the reactive interaction. An "inner" region generally arises in the partner's configurations where chemical interactions (*e.g.*, covalent bonding and steric repulsions) are of similar, or somewhat greater, strength than the long-range interactions (*e.g.*, multipole, dispersion, and induced interactions). At the high temperatures typical of the combustion environments only the inner region is deemed to be important while, in contrast, in the low-temperature limit (of importance in interstellar chemistry) the outer state region also acquires significant relevance, as we shall further discuss below. The transition from a dominant outer 'transition state' to a dominant inner 'transition state' generally takes place quite gradually at temperatures of the order of 100 K. As a result, both states are expected to play a significant role at the temperatures of the molecular clouds where the present types of anions have been sighted.

We therefore start with a description of the formation reaction that should follow, in a reduced-dimensionality picture, the two dominant variables of the reaction in eqn (2), *i.e.* the distance of the H^- partner approaching co-linearly either of the H atoms at the end of the $HC_{10}H$ neutral chain, and the one describing the detachment of that terminal H-atom from the neutral chain, thus forming the H_2 neutral product with the incoming H^- partner, leaving behind the anionic product. Our previous calculations, mentioned earlier for other, similar ion–molecule reactions,[14] had in fact shown that the relative distances and the linear geometries do not change much from the initial neutral out to the final anionic molecule. Hence, we can focus on a sort of simplified treatment which analyses the reactive evolution coming from those two reacting coordinates. Our calculations therefore carried out the numerical optimization of the C–H distance for every H–H distance, using MP2 with aug-cc-pVDZ basis and then a single point CCSD(T) energy calculation with cc-pVQZ basis. The H–H distance hence being obtained as single-point optimized energies following the method mentioned earlier for the two isolated molecules: neutral and anionic. The C–H distances went from about 1.07 Å, the equilibrium value, out to 2.92 Å while the corresponding H–H distance was varied from 20.0 Å down to 0.60 Å.

Table 2 summarizes the energies of all fragments involved in the reaction, including in a separate column the zero point energy (ZPE) correction, and the exothermicity of the anionic reaction which starts from the neutral radical.

A schematic presentation of the spatial evolution of the minimum energy path (MEP) energies is also reported in Fig. 1, where the two reactive coordinates mentioned earlier are shown within the short-range region of the stronger reactive

Table 2 Computed energy values associated with the fragments discussed in the present reaction model. The total energies of the reactants and products are also reported

cc-pVQZ	$E(CCSD(T))$/a.u.	$E(ZPE_{corrected})$/a.u.
Energy of the fragments		
$HC_{10}H$	−381.330672	−381.266064
H^-	−0.506399	−0.506399
HC_{10}^-	−380.764713	−380.711767
H_2	−1.173773	−1.163476
Energy products (P) and reactants (R)		
R: $HC_{10}H + H^-$	−381.837071	−381.772463
P: $HC_{10}^- + H_2$	−381.938486	−381.875243
ΔE/eV	−2.76	−2.80

interaction. One clearly sees there that these reaction coordinates show strong exothermic behaviour and the absence of any reaction barrier along the descent to the product region.

If one now further looks at a 2D presentation, given by the curve of Fig. 2, one also sees that the geometry changes along the minimum energy path, as seen before but now presented more clearly. While the H_2 molecule gets formed down to its equilibrium value (at about 0.75 Å), we see that the terminal C-atom rapidly loses its H-atom to the newly obtained hydrogen molecule and the corresponding C–H distance becomes much larger.

We report in Fig. 3 another pictorial view of the energy evolution in the present reduced-dimensionality model, whereby one sees that, as the H^- partner approaches from about 4.0 Å from the outer H-atom of the $H–C_{10}H$ radical, the total energy changes very little until about 1.5 Å, after which distance the energy drops rapidly while the two H atoms form the H_2 neutral molecule (at the bottom of the well) at a relative distance of about 0.75 Å between the outgoing hydrogen atoms.

One clearly sees there that the formation of the H_2 molecule corresponds to the energy minimum of the reaction, where the residual anion $C_{10}H^-$ has moved away to about 3.0 Å as shown by the structure of the energy minimum already reported by Fig. 1 and 2.
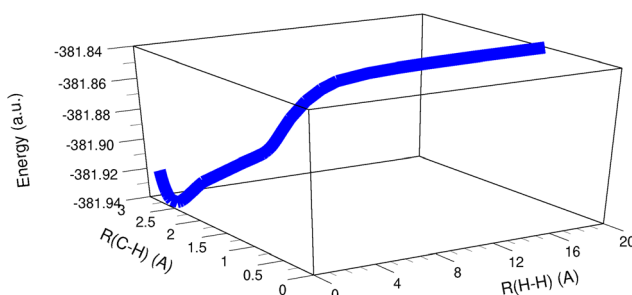

Fig. 1 Plot in 3D of the minimum energy path (MEP) obtained from the geometry optimization calculations of the initial input points along the two reactive variables. The latter are: $R(H–H)$, the distance between the incoming H anion and the terminal H of the radical partner, and $R(C–H)$, the distance within the radical partner between the end C-atom and its bonded H-atom. See text for further details.

This journal is © the Owner Societies 2025

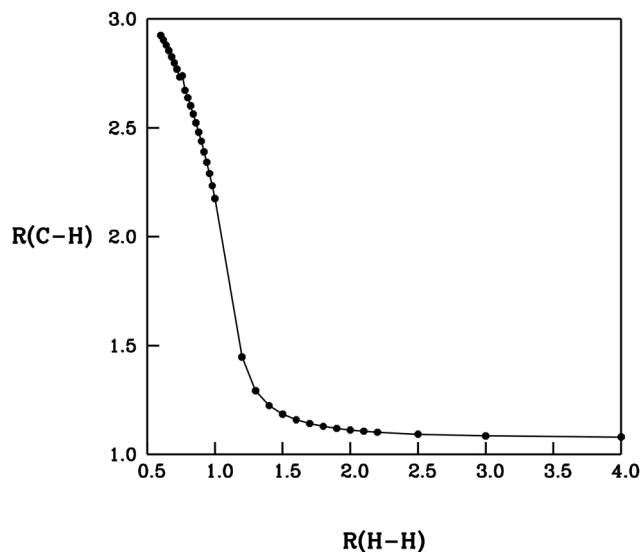*Phys. Chem. Chem. Phys.*, 2025, **27**, 21231–21243 | **21233**

Fig. 2 Plot of the bond length evolutions along the MEP energy shape for the newly formed H_2 molecule and the breaking of the C–H terminal bond in the radical partner (all distances in Å). The R(C–H) distance is that of the terminal end of the radical partner and the R(H–H) distance involves the incoming H^- reagent and the terminal H of the neutral radical. See text for further details.

Fig. 4 Evolution of the extra negative charge on the incoming H^- atom as it approaches the neutral radical and the H_2 neutral molecule is formed while the negative charge moves onto the product anion (not shown). The R(H–H) variable shows the distance between the H anion and the terminal H atom of the neutral. All distances in Å. See main text for further details.
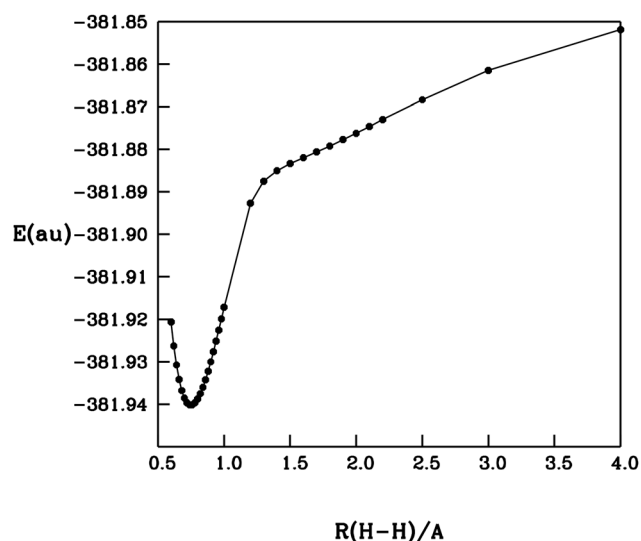

Fig. 3 Detailed energy region around the products' formation. The minimum energy corresponds to the equilibrium geometry of the newly formed H_2 molecule with the molecular anion located further away. Distances in Å and energies in a.u. The R(H–H) distance is the same as in Fig. 2. See main text for further details.

To further follow the intermediate steps along the 2D modeling of the reaction, we report in Fig. 4 the evolution of the initial negative charge on the approaching H^- partner as the molecular anion is being formed. The results originate from the approximate picture provided by the localized Mulliken charges between the reaction partners. One sees there that the reacting H^-, when far away from the neutral partner, carries a
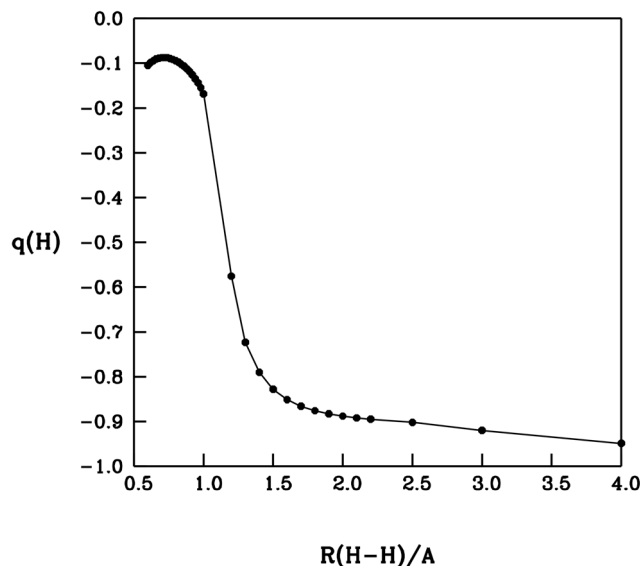
whole extra charge close to -1.0, while it starts to lose that extra charge as it comes closer to its neutral partner, *i.e.* from about 1.5 Å. By the time the H_2 molecule is formed with its R_{eq} around 0.74 Å the extra charge has moved onto the product anion, leaving the molecular H_2 product as largely neutral.

2.3 The anisotropic interaction with He atoms

Whenever one wishes to carry out detailed analysis of the column densities of a given species in dark molecular clouds (DMC), in order to compare the observation with the results from modeling data, it is important to assess as best as possible the validity of local thermal equilibrium (LTE) or a departure from it (non-LTE), depending on the relative significance of collisional energy transfer effects with respect to the radiative emission.[18]

To this end we have therefore also embarked on the direct calculations of the energy-transfer collision cross sections involving the rotational levels of the anion molecule interacting with one of the most common partners in the DMC environments: the He atom, a simpler case than the interaction with another common component, the H_2 molecule. A study of the energy transfer collisions with the hydrogen molecule using a 4D interaction potential for the quantum dynamics will be reported in later work, also in preparation in our group, also including different ISM anions.

We employed the equilibrium geometry of the isolated anionic molecule and constructed a 2D interaction potential using Jacobi coordinates, (R, θ), of the molecule with respect to the neutral atomic partner. The angle values went from $0°$ (on the H side) to $180°$ (on the C side) at intervals of $5°$, while the radial values went from about 8.0 Å to 15.0 Å at intervals of 0.1 Å. The total number of *ab initio* points was 5.400 and a long-

range (LR) form of interaction, to be discussed later, was employed at the larger distances required for the quantum scattering calculations (see below).

Note that the long, linear structure of the anionic species, and hence the location of the center-of-mass at the large distance mentioned earlier, are responsible for the interaction becoming highly repulsive already at fairly large distances of the atomic partner's approach to the center of mass (c.o.m.). We found that the actual radial range of the fitted potential gets closer to the c.o.m. for some of the angles needed in the scattering calculations, while staying further away for some of the others. Since the *ab initio* computed points are not symmetrically distributed along the collision coordinate, but depend on the entrance angle of the He atom, the ensuing lack of points at short distances has to be improved and extended. We did that by extrapolating with an exponential function for every angle up to 2 Å with respect to the c.o.m. In order to generate a uniformly regular grid of points, spline functions were used on the *ab initio* and on the extrapolated points to produce a total of additional 131 distance (R) points along the 37 angles (θ), summing up to a total of additional 4978 points, further fitted to generate the final PES. The presence of 'ghost points' at very short distances is due to the extremely large energy values which accumulate over short radial intervals. This causes mathematical instabilities when trying to fit them *via* an analytical function. To overcome this problem, we scaled the points by applying the simple procedure implemented by ref. 19 and already used by us in similar systems.[20–22] It has the advantage that one can now reproduce the original *ab initio* points in the lower energy range of the PES (the most relevant range for the scattering calculations) while one only scales the higher energy values that would not be sampled during the scattering events at low collision energies. Thus, one can write the following sequence,

$$
\begin{aligned}
V_s &= V_a & \text{for } V_a \leq V_{T1}, \\
V_s &= V_{T1} + (V_{T2} - V_{T1})S\left(\frac{V_a - V_{T1}}{V_{T2} - V_{T1}}\right) & \text{for } V_{T1} < V_a \leq V_{T2}, \\
V_s &= V_{T1} + \frac{2}{\pi}(V_{T2} - V_{T1}) & \text{for } V_a > V_{T2},
\end{aligned}
$$

where V_s is the scaled potential, V_a is the *ab initio* energy and V_{T1} and V_{T2} refer to two threshold energy values, which for this particular case are 4700 cm^{-1} and 12 000 cm^{-1}, respectively.

The switching function is given by the S function defined as

$$
S(x) = \frac{2}{\pi}\sin\left[\frac{\pi}{2}\sin\left(\frac{\pi}{2}x\right)\right] \tag{3}
$$

and it guarantees the proper transition between the three different scaling windows.

In the procedures employed for solving the coupled-channel (CC) scattering equations, it is usually convenient to expand the interaction potential $V(R,\theta)$ into orthogonal angular functions.[23–26] Hence, for a quantitative evaluation of the spatial anisotropy around the $C_{10}H^-$ linear anion it is useful to represent the raw, 2D grid of points from the *ab initio* calculations in terms of the familiar Legendre polynomials in their standard (R,θ) form. In the case of the calculations

discussed above by using the 3034 'scaled points' we were able to expand the PES *via* the usual orthogonal Legendre polynomials for the θ angle:

$$
V_{\text{FIT}} = V(R,\theta) = \sum_{\lambda=0}^{\lambda_{\max}} V_\lambda(R)P_\lambda(\cos\theta). \tag{4}
$$

The fitted potential is restricted to a specific range of R values and therefore we extrapolated to an asymptotic form to describe the long-range interaction forces. The analytical form used for the main long-range contribution is

$$
V_{\text{LR}} = -\frac{\alpha_0}{2R^4} + \left(\frac{2\alpha_0\mu}{R^5}\right)\cos\theta, \tag{5}
$$

where $\alpha_0 = 1.41a_0^3$ is the polarizability of the He atom and the calculated dipole moment of the long-chain anion was found by us to be 14.265 Debye, not far from the value of 15.2 D suggested by ref. 27, also from calculations.

To ensure the smooth transition between the V_{FIT} fitted PES (eqn (4)) and the V_{LR} long-range term (eqn (5)) in the construction of the V_f final PES, the switching procedure which was already used for C_5N^-/He[28] has also been implemented for the present, longer chain anion:

$$
V_f = f_s V_{\text{FIT}} + (1 - f_s)V_{\text{LR}}, \tag{6}
$$

where the switching function is

$$
f_s(R) = \frac{1}{e^{\frac{(R-R_0)}{\Delta R}}+1} \tag{7}
$$

with $R_0 = 18.5$ and $\Delta R = 1.2$ Å.

A pictorial view of the spatial shape of the interaction forces for $C_{10}H^-$/He is reported in Fig. 5, where the energy isolines are around the linear, rod-like structure of the anionic partner. This pictorial view of the interaction indicates that the deepest well of the attractive region is located away from the terminal atoms and closer to the central C-atoms of the chain.
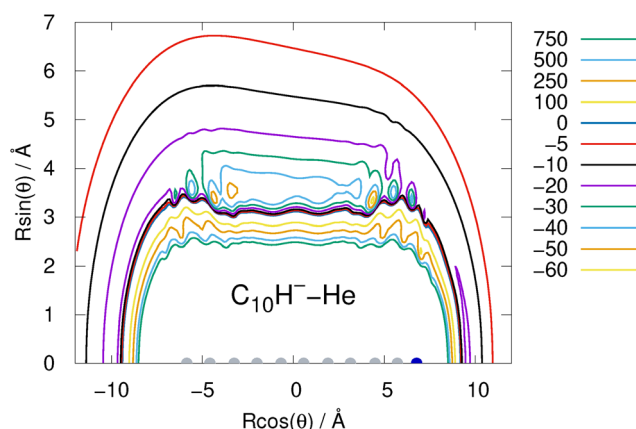

Fig. 5 Pictorial representation of the spatial features of the interaction between the $C_{10}H^-$ partner and the He atom. The first C atom is on the extreme left of the figure, while the end H atom is on the extreme right along the same x-axis. See main text for further details.

This journal is © the Owner Societies 2025

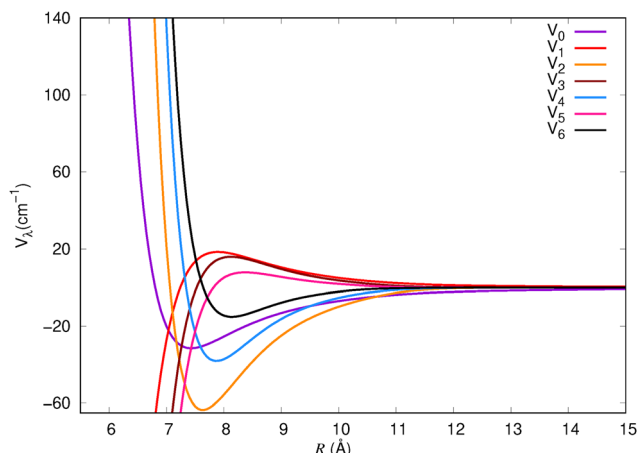*Phys. Chem. Chem. Phys.*, 2025, **27**, 21231–21243 | **21235**

Fig. 6 A pictorial view of the lower radial multipolar coefficients for the interaction potential energy surfaces between the $C_{10}H^-$ anion and the He atom. See main text for further comments.

Additionally, the radial features of the lower terms of the multipolar expansion of the 2D interaction are further presented in Fig. 6. One sees now that the dominant anisotropic coupling between rotational levels chiefly comes from the $\lambda = 2$ and 4 radial coefficients, which show a marked attractive well region at the shorter distances, with the $\lambda = 6$ term also exhibiting a shallow attractive well. The effects from such angular couplings will be further discussed below when presenting the inelastic cross sections and rate coefficients. The actual calculations employed λ values up to $\lambda = 30$.

3 The quantum dynamics methods

3.1 The VTST reactive quantum method

The features of the reactive interaction, discussed in Section 2.2, have told us that the reduced-dimensionality reaction follows an exothermic path with no barrier from reagents to products. Furthermore, the data discussed in the figures in Section 2.2 tell us that the most energetically-favored approach would be along the collinear MEP during which the H_2 formation occurs at relatively short distances between partners (between 2.5 and 3.0 Å) and is concurrent with the occurrence of the $C_{10}H^-$ ionic formation.

We have therefore decided that it would be reasonable to try and model the reaction rates for the formation of the present anion by using the variational transition state theory (VTST) approach, a well-suited model for exothermic chemical reactions without a barrier: *e.g.* see ref. 29, within the reduced dimensions suggested by the RPES features produced by our calculations and described earlier. As a matter of fact, we have recently employed the VTST treatment in order to produce the reaction rates of similar C-bearing chains which included a terminal –CN group: *e.g.* see ref. 13 and 9, where we found them to be in line with the expected magnitude of this type of reaction.

More specifically, the VTST scheme allows one to estimate the transient 'transition state' (TS) partition functions as being

given by the direct product between the conserved modes during reactions, Q_{cons}, and the translational mode partition function, Q_{trans}, along which the optimal reaction is occurring:

$$Q^{\ddagger}(T) = Q^{\ddagger}_{cons}(T)Q^{\ddagger}_{trans}(T) \tag{8}$$

For the present modeling of our reaction, the most favored exothermic path takes place along the collinear MEP configuration so that the dominant translational mode will be along the $HC_{10}H\cdots H^-$ reaction coordinate. The present approach will consider the exponential factor of the TST formulation as being equal to unity since in a barrierless process the enthalpy of the transition state is equal to zero.[29] The corresponding pre-exponential factor of the VTST scheme is then the usual canonical formulation of the reaction rate coefficient:

$$k_{can}(T) = \frac{k_B T}{h} \frac{Q^{\ddagger}_{HC_{10}H-H^-}(T)}{Q_{HC_{10}H}(T)Q_{H^-}(T)} \tag{9}$$

where k_B is the Boltzmann constant and h is Planck's constant. The $Q^{\ddagger}_{HC_{10}H-H^-}$ is the molecular partition function of the reaction complex, which is variationally minimized along the MEP at each temperature. $Q_{HC_{10}H}$ and Q_{H^-} are the molecular (atomic) partition functions (PFs) of the two reagents. For the long chain of the radical the individual PFs are optimized within a 3D normal-modes formulation along the MEP. Both high-frequency and low-frequency modes are treated as normal modes during the evolution along the MEP path. The r.h.s. of eqn (9) is therefore also T-dependent, as it should be.

In order to employ the factors defined in eqn (9) to search for the lowest-positioned reactive path, one needs to generate the minimum values of the partition functions involved along the pseudo-2D process we are considering, *i.e.* along the R_{H-H} and R_{H-C} distances, for a broad range of the angle θ_{HHC} between the reacting fragments. At all temperatures considered in the present study, the searches for minimum values of the partition functions yielded the collocation of the TS along the $\theta_{HHC} = 180°$, a result which thus allows us to compute the short-range part of the reaction rate using the initial shapes of the radical partner (its optimized PFs) along the reaction MEP configuration. This model basically assumes that, for the present type of reaction, the formation of a transition-state complex along the exothermic energy path from reactants to products controls the efficiency of product formation *via* the relative energetic between the partition functions of that complex and those of the initial reactants.

Since in the present study we are interested in the low-T behaviour within the interstellar DMCs where the anion has been sighted, we have also implemented separately the long-range formulation of eqn (9) as presented in detail by Klippenstein *et al.* in ref. 30. In that work, the standard transition state theory has been extended to including the case of long-range potential forms (see their eqn (1)) given as:

$$k_{LR}(T) = C_1 \mu^{-1/2} V_0^{2/3} T^{-1/6} \tag{10}$$

where C_1 is a dimensionless proportionality constant, which is 2.07 for the charge–quadrupole interaction, μ is the reduced

21236 | *Phys. Chem. Chem. Phys.*, 2025, **27**, 21231–21243

This journal is © the Owner Societies 2025

mass of the reagents, V_0 is the strength of interaction between the fragments and it is $V_0 = eQ$, where e is the electron charge, and Q is the quadrupole of $HC_{10}H$, which has been calculated (B2PLYP/cc-pvdz) as $Q_{xx} = Q_{yy} = 57.84$ and $Q_{zz} = 17.38$ Debye Å.

We carried out the modeling of the exothermic reaction (2), starting from the low-T region and extending it up to room temperature, by using independently two different formulations of the TST: one including the role of the long-range (LR) forces along the MEP path and another treating the TS complex chiefly within the shorter range action *via* the variational method of the VTST modeling. The results of the calculations will be given in the next section and the implications of our finding will be analysed there.

3.2 The inelastic coupled channels method

When one is interested in the non-reactive dynamics involving only the rotational channels of the target anion, as is our present case, then the total scattering wave function can be expanded in terms of asymptotic target rotational eigenfunctions (taken to be spherical harmonics) whose eigenvalues are given by $B_e j(j + 1)$ where B_e is the first rotational constant mentioned earlier for the present systems.[23–26] Its value was taken from the above references as 0.010054 cm^{-1}. The channel components for the CC formulation are therefore expanded into products of total angular momentum eigenfunctions and of radial functions.[23] The latter are in turn the elements of the solutions matrix which appear in the familiar set of coupled, second order homogeneous differential equations:

$$\left(\frac{d^2}{dR^2} + \mathbf{K}^2 - \mathbf{V} - \frac{\mathbf{l}^2}{R^2}\right)\Psi = 0 \qquad (11)$$

where $[\mathbf{K}]_{ij} = \delta_{i,j} 2\mu(E - \varepsilon_i)$ are the matrix elements of the diagonal matrix of the asymptotic (squared) wavevectors and $[\mathbf{l}]_{ij} = \delta_{i,j} l_i(l_i + 1)$ is the matrix representation of the square of the orbital angular momentum operator. This matrix is block-diagonal with two sub-blocks that contain only even values of $(l' + j')$ or only odd values of $(l' + j')$.

The scattering observables are thus obtained in the asymptotic region where the log-derivative matrix is given in terms of free-particle solutions and unknown mixing coefficients. For example, in the asymptotic region the solution can be written as:

$$\Psi = \mathbf{J}(R) - \mathbf{N}(R)\mathbf{K} \qquad (12)$$

where $\mathbf{J}(R)$ and $\mathbf{N}(R)$ are matrices of Riccati–Bessel and Riccati–Neumann functions. At the end of the propagation, from the log-derivative matrix one obtains the $\mathbf{K}$ matrix by solving the following linear system:

$$(\mathbf{N}' - \mathbf{Y}\mathbf{N}) = \mathbf{J}' - \mathbf{Y}\mathbf{J} \qquad (13)$$

and from the $\mathbf{K}$ matrix the S-matrix yields the individual state-to-state cross sections.

The latter inelastic observables are given by the following equation, for state-to-state rotational inelastic transitions:

$$\sigma_{j \to j'} = \frac{\pi}{(2j+1)k_j^2} \sum_J (2J+1) \sum_{l,l'} \left| \delta_{lj,l'j'} - S^J_{lj,l'j''} \right|^2. \qquad (14)$$

In the present calculations we first generated the necessary state-to-state rotationally inelastic cross sections and, once these quantities were known, the required rotationally inelastic rate coefficients $k_{j \to j'}(T)$ were evaluated as the convolution of these cross sections $\sigma_{j \to j'}$ over a Boltzmann distribution of the relative translational energy values between partners (E_{trans}):

$$k_{j \to j'}(T) = \left(\frac{8}{\pi \mu k_B^3 T^3}\right)^{1/2} \int_0^\infty \sigma_{j \to j'}(E_{\text{trans}}) \cdot E_{\text{trans}} \cdot e^{-E_{\text{trans}}/k_B T} dE_{\text{trans}}$$

$$(15)$$

The reduced mass for the $C_{10}H^-$/He systems is (in units of amu) 3.4467, while the rotational constant value employed was 0.010054 cm^{-1}. The individual rate coefficients were obtained at intervals of 1 K, starting from 10 K and going up to 50 K. The scattering calculations for this large anion were carried out using the MOLSCAT suite of codes[31,32] with the full Coupled Channel (CC) treatment of the angular momenta coupling, as discussed earlier.

Briefly, the maximum value of J_{TOT} was 90 at the highest collision energies and was reduced to 70 near the threshold energies. The range of integration went out up to $R = 300$ Å and started at $R = 2.0$ Å. The convergence checks of the results indicated an accuracy of the cross sections around 2–3%. The spacing of the energy points (in cm^{-1}) for the cross section calculations varied from 0.00001 up to 10.0 cm^{-1} with steps that increased from 0.00001 up to 1.0 cm^{-1}. From 20 cm^{-1} up to 90 cm^{-1} with steps of 10 cm^{-1}, from 100 to 300 cm^{-1} with steps of 25 cm^{-1}. We further found that, for the studied transitions, to include rotational states up to $j_{\text{max}} = 40$ was sufficient, with the chosen maximum value of J_{TOT} mentioned earlier.

4 Discussion of results

4.1 Anion's formation reaction from H$^-$ and the neutral radical

As presented in the previous section, we have carried out a reduced-dimensionality study of the formation reaction (2) of the $C_{10}H^-$ anion by computing the reactive interaction of H$^-$ and the neutral radical $HC_{10}H$, a species also detected in the same ISM environment.[7]

We have followed the evolution of the MEP from reactants to products, see Section 2.2, and generated the variationally minimized PFs for all the degrees of freedom of the long radical partner and of its anionic product as detailed in Section 3.1. We have then employed the long-range formulation of the TST as in eqn (10) (the LR-TST method) to further explore the low temperature region. Basically, we employ the TST approach
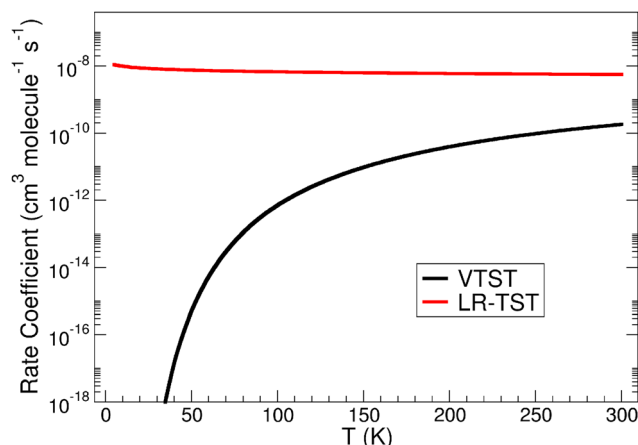
This journal is © the Owner Societies 2025

Phys. Chem. Chem. Phys., 2025, **27**, 21231–21243 | **21237**

Fig. 7 Reaction rates computed using the VTST (black curve) and LR-TST (red curve) methods discussed in the main text. See there for further details.

independently within two different approaches, *i.e.* we employ the variational use of the PFs in the short-range region to produce rate coefficients within the VTST method. Further, we employ the multipolar formulation of the LR forces along the same MEP to obtain the LR-TST rate coefficients.

The results of our calculations are reported in Fig. 7, where the range of temperatures goes from the low-*T* of the dark molecular clouds (DMC) regions up to room temperature. It is interesting to note that the LR-TST results, given by the red curve, appear to depend very little on the *T* values and produce over the whole range substantial rate coefficients of the order of 10^{-8} cm^3 molecule^{-1} s^{-1}. This result turns out to be very close to the room-temperature values of reaction rate coefficients found a while ago from experiments on similar systems,[33] as we shall further discuss in the next subsection. On the other hand, using the VTST formulation which involves only the short-range region of the interaction, as discussed earlier, yields very small rate coefficients at low-*T*, and only gets closer to the red curve results once room temperatures are reached.

One can therefore conclude from the present modeling of the formation reaction (2) that the inclusion of LR forces to the description of the TS interactions becomes a crucial ingredient for making the reaction to exhibit fairly large rate coefficients down to the low temperatures of interest.

In order to make our present findings more usable within general chemical modelings of the formation of the present anion, the rate coefficients from the red curve in Fig. 7 are represented through a formulation commonly employed within various chemical databases. This is obtained by the parameters reported in Table 3.

Table 3 Parameters of the fit of the LR-TST rate coefficient carried out using the following equation: $k = \alpha \left(\dfrac{T}{300} \right)^{\beta} e^{-\gamma/T}$

| α (10^{-10} cm^3 molecule^{-1} s^{-1})	β	γ (K)
9.2116	0.1226	3.1166

To make further contact with the few available experimental data, it is worth mentioning here that fairly old measurements of reaction rates from eqn (2), and involving smaller chains like HCN and HC$_3$N,[34] reported formation coefficients at temperatures around 300 K of the order of 10^{-8} to 10^{-9} cm^3 molecule^{-1} s^{-1}. The computed rate coefficients we have obtained from the present study, and seen in Fig. 7 (both the red and black curves), are reaching that large rate coefficient value at room temperature. This agreement within one order of magnitude with earlier results for similar systems (none exist for the present reaction) supports the realistic quality of the present modeling, which then gives reasonable estimates at room temperatures for existing measurements in similar anionic chains.

It is also interesting to note that in recent work that put forward various formation reactions for the present anion,[7] it was suggested that the main production route of these anions would be through radiative electron attachment (REA) to the neutral fragment precursor:

$$\text{e}^- + \text{C}_{10}\text{H} \rightarrow h\nu + \text{HC}_{10}^- \qquad (16)$$

Although no experimental evidence exists as yet on measured values of those rate coefficients, we however know from more recent, sophisticated calculations on smaller anions like C$_4$H$^-$ and others,[35] that the electron attachment rates were found to be rather small: of the order of 10^{-16} cm^3 molecule^{-1} s^{-1} at the temperature of interest. Hence, such values would be too small to be playing a significant role in the chemical formations of this class of anions. On the other hand, the present results from the chemical path analyzed here indicate that this route could instead provide significant rate coefficients for the formation of the longest linear polyyne detected in molecular clouds.

Another possible production route was also surmised in earlier studies, involving reactions between longer carbon-chain anions and atomic oxygen,

$$\text{O} + \text{HC}_{11}\text{H}^- \rightarrow \text{CO} + \text{HC}_{10}^- \qquad (17)$$
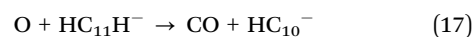
However, these rate coefficients are not yet known accurately enough to be reliably included in chemical networks, while the abundance of oxygen as a reaction partner is still considered to be marginal in the DMC under consideration.[3,27]

It is also interesting to note that there are two further product channels suggested a while ago for the destruction reactions between carbon-chain anions and atomic hydrogen,[3] involving either associative electron detachment:

$$\text{H} + \text{C}_n\text{H}^- \rightarrow \text{e}^- + \text{H}_2\text{C}_n \qquad (18)$$
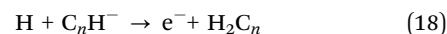
or fragmentation in the case of the longer chains:

$$\text{H} + \text{C}_{10}\text{H}^- \rightarrow \text{C}_2\text{H} + \text{HC}_8^- \qquad (19)$$
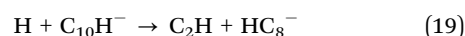
In that work all these rates were estimated to be, but only at room temperatures, of the order of 10^{-9} cm^3 molecule^{-1} s^{-1}. Hence, in the low-*T* regimes of interest here we have no indication from any source that the values of such reaction rates would be large enough to be relevant.

21238 | *Phys. Chem. Chem. Phys.*, 2025, **27**, 21231–21243

This journal is © the Owner Societies 2025

In conclusion, what we have shown in the study reported above is that the H$^-$-linked route to formation of the title anion would be yielding reaction rate coefficients which are markedly larger than the best estimates so far on the radiative electron attachment routes[35] or from other chemical reactions. Hence, although the issue of knowing the possible H$^-$ abundances is still an open question, we suggest that in the chemical modeling of the evolutionary studies on the present class of anions, it would be reasonable estimating its rate coefficients of formation by using the results obtained by the reduced-dimensionality modeling we have developed in the present study.

4.2 Rotational inelastic cross sections and rate coefficients from collisions with He

In Section 3.2 we have discussed in some detail the numerical solutions for the quantum scattering equations of collisions between the title linear anion and the neutral He partner, a species present in the interstellar environment where $C_{10}H^-$ has also been found, as discussed in the Introduction.

The relative size and energy dependence of the computed inelastic cross sections are reported, as examples of the many transitions we have obtained, for the cooling (de-excitation) processes in the three panels of Fig. 8. We report, on a log scale, in each of them transitions involving Δj values of -1 (top panel), -2 (middle panel) and -3 (bottom panel).

The panels of Fig. 9 deal with the corresponding rotational excitation calculations.

The cross sections reported in those panels show for all processes the presence of oscillations near the threshold converging to a uniform behaviour at the higher energies over the rest of the examined ranges. Given the relative strength of the ionic interaction, and because of the small energy spacing of the rotational states for this long linear partner with a very small rotational constant (see earlier discussions), we have for this system a markedly strong coupling between several rotational states during the collision interaction. Hence, for energies close to the threshold we expect the occurrence of several closed channel effects leading to Feshbach resonances, as well as several shape resonances occurring for different values of the contributing J_{TOT} angular momentum.[23] The detailed analysis of such resonances is, however, outside the scope of the present work, although we employed a fairly dense energy grid near thresholds to make sure that we would include all the contributions of such cross section peaks, as they will obviously affect the values of the ensuing rate coefficients we calculated from them, as further discussed below.

Broadly speaking, we see as well that fairly similar values are exhibited within each figure by the excitation and the cooling transitions. However, and more specifically, we further notice that the excitation cross sections reported by Fig. 9 are somewhat smaller than the corresponding cooling processes given by the panels of Fig. 8. This is due to the microscopic reversibility effects which work at reducing the relative sizes of the excitation transitions in comparison with the de-excitation ones. Finally, the different strengths shown by the multipolar coefficients in eqn (4), and reported in Fig. 6, should be
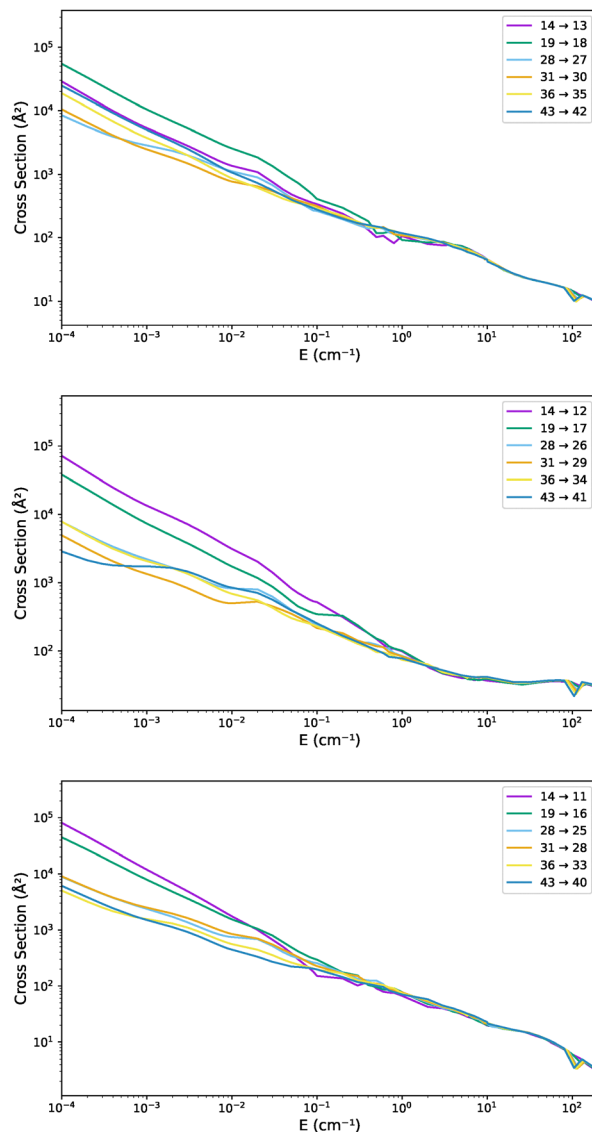

Fig. 8 The panels of this figure report de-excitation rotational cross sections for the title anion of this work in collision with He atoms. The top panel shows $\Delta j = -1$ transitions, while the middle panel shows the $\Delta j = -2$ processes and the bottom panel the $\Delta j = -3$ de-excitations. See the main text for further comments.

considered responsible for the much larger inelastic transitions exhibited by the data in the middle panel of Fig. 9: the presence of a large $\Delta \lambda = 2$ coupling coefficient drives here the size of these cross sections.

By applying the numerical quadrature given by eqn (14) we have obtained the corresponding rate coefficients over a range of temperature of interest for the astrophysical environment where this molecule was found. The results reported by Fig. 10 show, as examples, the range of values for the collision rates involving the excited rotational states indicated by the observational data mentioned earlier and for transitions with $\Delta j = 1$. Once again we find that the excitation rate coefficients involving the lower levels are larger than those where higher rotational levels are involved. This is due to the different values of
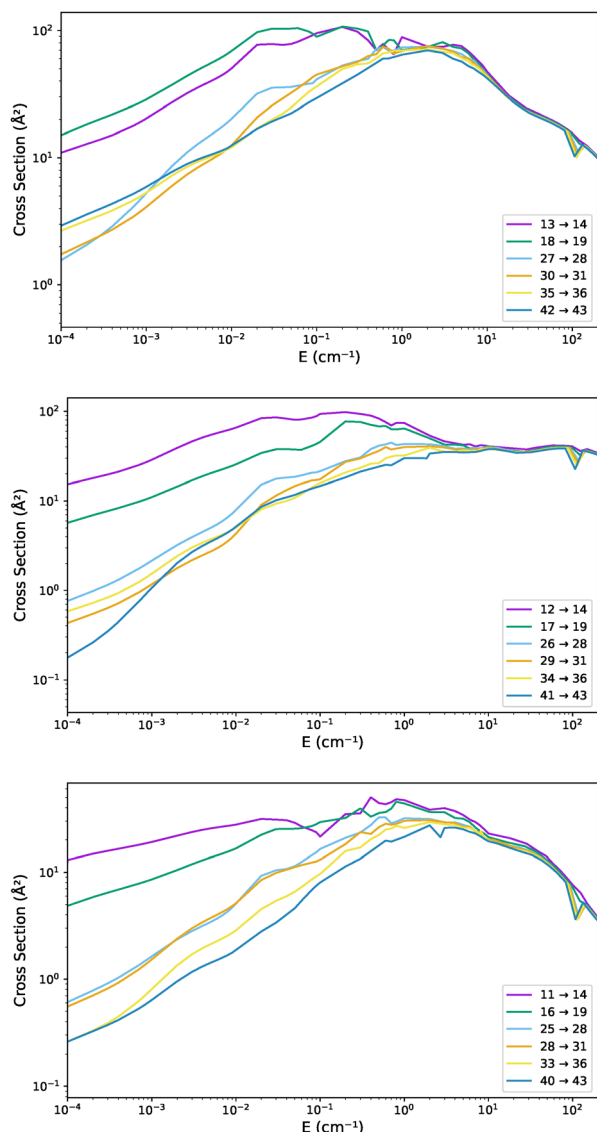
Fig. 9 The panels of this figure report excitation rotational cross sections for the title anion of this work in collision with He atoms. The top panel shows $\Delta j = +1$ transitions, while the middle panel shows the $\Delta j = +2$ processes and the bottom panel the $\Delta j = +3$ excitations. See the main text for further comments.
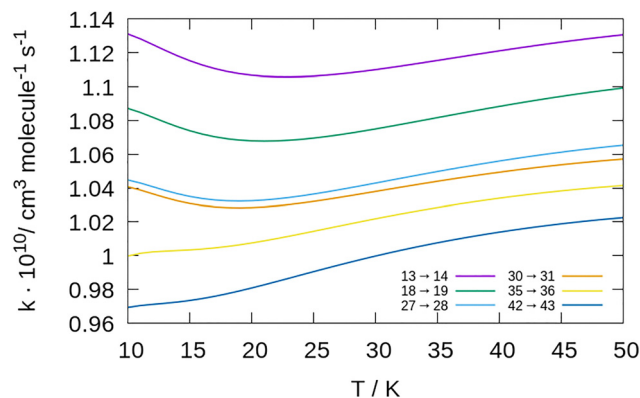

Fig. 10 Computed rotationally inelastic excitation rate coefficients for the title anion in collision with He atoms, using the quantum method discussed in Section 3.2. See there for further details. The colour code is the same as in Fig. 9.

also reported in the present study. We had found there that the involved levels would provide density estimates of about 10^5 cm^{-3}, which is typically the density in circumstellar gas and star-forming regions. Therefore, in low- to moderate-density molecular environments, high rotational levels can possibly achieve near-LTE conditions due to the large rate coefficients.

To assess more accurately how realistic are our estimates of level populations to model anionic line emissions, the rate coefficients calculated in this work should be compared with other systems in order to assess the corresponding efficiency of the collisional cooling driven by He as a partner. This is carried out in the following subsection.

The size of the presently computed inelastic rate coefficients, however already suggest that using the local thermal equilibrium (LTE) description for the populations of the rotational states of the present long chain may be a good approximation in environments like the TMC-1, since the He collision partner is seen here to yield fairly large rate coefficients and therefore can generate critical density values close to the known population densities in that environment.
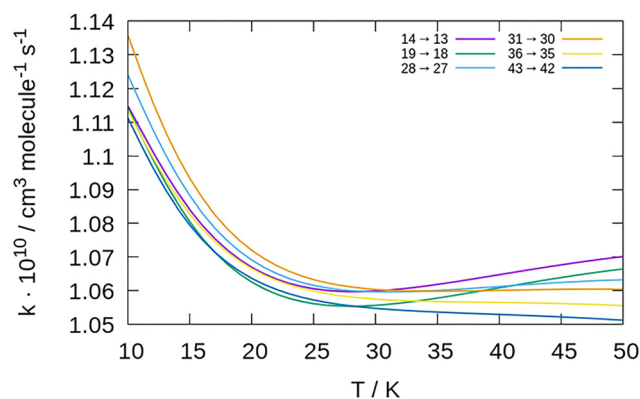
the multiplicity factors being present between lower-lying rotational levels, hence affecting the energy gaps between such levels. On the whole, however, we see that the present rate coefficients range in values that are largely close to 10^{-10} cm^3 molecule^{-1} s^{-1}. Such values are in line with earlier calculations for other long linear polyyne anions.[14]

In Fig. 11 we report rate coefficient values associated with cooling processes among the same levels discussed in Fig. 10. These rates, as also found for the original cross sections, are slightly larger in size but follow the same trends seen for the excitation processes, which finds the smaller rate coefficients to be associated to transitions among the higher rotational states of the anion.

In our earlier work on linear anions[36] we had also estimated the values of the critical densities, involving the excited levels

Fig. 11 Computed rotationally cooling collision rate coefficients for a sampling of rotational states discussed in the main text, where the quantum calculations details are also given. See there for further details. The colour code is the same as in Fig. 8.

21240 | *Phys. Chem. Chem. Phys.*, 2025, **27**, 21231–21243

This journal is © the Owner Societies 2025

4.3 Comparison with a shorter linear anion: C_6H^-

The data reported by Fig. 12 compare the present rate coefficients, involving transitions between two of the lower rotational levels, with those obtained earlier for the C_6H^- anion.[37] In the case of that shorter chain, the rotational constant used was 0.045927 cm^{-1}, to be compared with the value of 0.010054 cm^{-1} we used here for the longer chain. We have already discussed earlier that a sort of propensity rule which can be extracted by comparing the relative magnitudes of inelastic cooling cross sections (and their corresponding rates) is that transitions involving larger energy releases yield larger rate coefficients. This is shown in Fig. 12 when we compare the dash-dotted (green and purple) lines associated with the lower transitions involving the $C_{10}H^-$ anion, with those given by the green and purple solid lines with thick dots, which are labeling the same transitions for the C_6H^- anion. These latter rate coefficients are markedly larger than the former, since they are associated with larger amounts of energy release in comparison with the case of the longer anionic chain. In Fig. 12 we also report for further comparisons some results for the same transitions but involving the CN^-, a system that exhibits a larger rotational constant: 1.87239 cm^{-1} (ref. 37) with respect to that of the present long carbon chain. As a consequence, we see that its cooling rate coefficients are the largest of the present selection of anions. These findings are in line with what we discussed before in terms of energy gaps between states and relative strengths of the interaction potentials.

The results reported by the two panels of Fig. 13 are also indicative of the differences in collision behaviour between the two carbon chains discussed already in Fig. 12. In the top panel of Fig. 13, in fact, we show cooling collision rates originating from the $j = 5$ rotational states of both anions, while the lower panel shows results of the same processes but starting from the $j = 10$ initial level of both anions. Given the similarities between the two chains we see that the relative magnitude and j-dependence are fairly similar for both anions. However, we
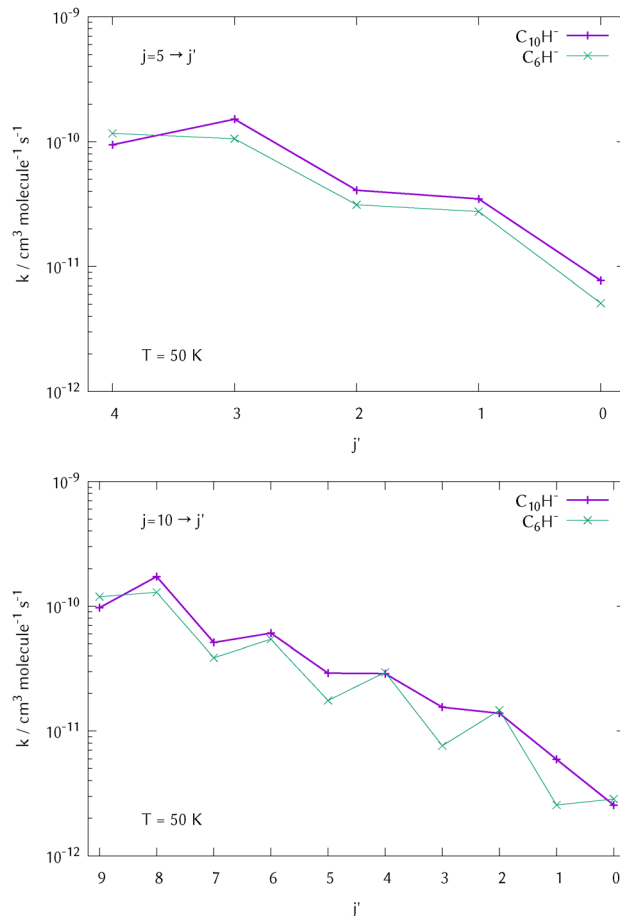

Fig. 13 The panels of this figure report de-excitation rotational cross sections for the title anion of this work in collision with He atoms and compares them with the same transitions for the C_6H^- anion also in collision with He atoms. The top panel shows cooling transitions from the $j = 5$ initial state, while the lower panel shows processes from the $j = 10$ initial level. See the main text for further comments.

also see that transitions involving the longer chain, with slightly smaller energy gaps between excited rotational levels, are yielding slightly larger cooling probabilities, in line with what we discussed earlier.

5 Present conclusions

In the study described in the previous sections we have investigated in some detail several features of the dynamics involving the longest C-bearing chain anion sighted thus far in ISM environments,[7] i.e. the $C_{10}H^-$ chain. By using quantum computational methods we have obtained indicators on the efficiency of its collision-controlled rotational state populations (at the observational temperatures of the ISM environments discussed in the Introduction section) by interaction with He atom, one of the more abundant atomic species present in the DMC environments. We have also investigated, by theoretical modeling, the rate coefficients for this anion to be formed by reaction of the H^- partner with the radical molecule $HC_{10}H$. In this latter case, we have considered a nearly linear reaction path
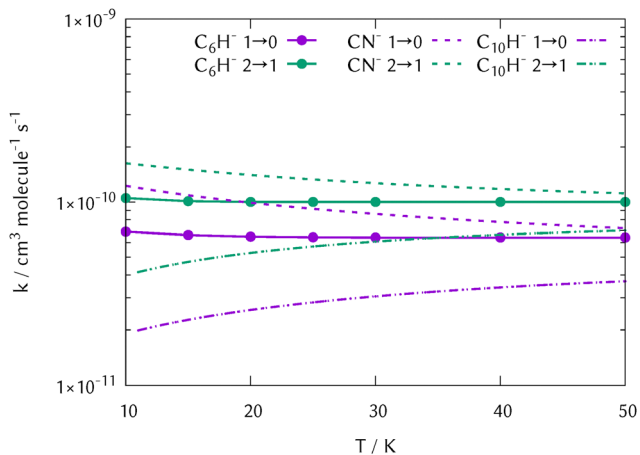

Fig. 12 Comparison between calculated inelastic rate coefficients for collisions of the $C_{10}H^-$ anion with He, and those obtained earlier in ref. 37 for the C_6H^- anion. Results for other species reported in ref. 37 are also shown. See the main text for discussion.

This journal is © the Owner Societies 2025

Phys. Chem. Chem. Phys., 2025, **27**, 21231–21243 | **21241**

using the variational transition state model discussed earlier in this paper. The modeling of this reaction has produced rate coefficients which, at the low temperatures of the ISM environment,[7] were found to be very large and in line with those observed at room temperatures for shorter chains.[9] The present modeling also found that the VTST approach, in order to produce realistic results in the low-T range, requires the inclusion of the correct long-range forces outside the region of the TS formation, a feature expected to play a role when dealing with exothermic reactions without a reaction barrier but with significant long-range interactions. Given the fact that the present formation reaction (2) is of interest at the lower temperature regions of the DMC conditions, our present results clearly suggest that the inclusion of the LR forces within the VTST treatment of the reaction becomes a significant component for yielding final rates of significant value.

The collision-controlled rotational state changes induced by the interaction with He atoms also turn out to be fairly large and therefore suggest that, due to the fairly small value of the rotational constant in the present long anionic chain, the overall condition for the rotational level populations in the present, highly excited rotational states would be close to an LTE situation.

We further compare the collision rate coefficients calculated in the present work with earlier findings from collision of the same longest chain with the H_2 partner and with the earlier behaviour for the inelastic rate coefficients involving the C_6H^- anionic linear chain, also in collision with the He partner. Such comparisons suggest that the present long chain would consistently yield rate coefficients which are somewhat smaller, albeit close to those from the shorter chain.

In conclusion, a combination of quantum inelastic dynamics and of quantum reactive modeling of its formation reaction provides in this study a variety of useful information on the chemical evolution of the longest carbon chain observed thus far in a Molecular Cloud.

Conflicts of interest

There are no conflicts of interest regarding this work.

Data availability

The data supporting this article are included as part of the supplementary information (SI). Supplementary information: inelastic rotational cross sections for collisions with He; inelastic rate coefficients for rotational processes from collisions with He; the multipolar coefficients for the nonreactive interaction with He; the original *ab initio* computed points for the reactive PES and the nonreactive PES. See DOI: https://doi.org/10.1039/d5cp02685g.

Acknowledgements

Notes and references

1 T. J. Millar, C. Walsh and T. A. Field, *Chem. Rev.*, 2017, **117**, 1765–1795.

2 A. Dalgarno and R. A. Cray, *Astrophys. J.*, 1973, **181**, 95.

3 N. Harada and E. Herbst, *Astrophys. J.*, 2008, **685**, 272.

4 M. C. McCarthy, C. A. Gottlieb, H. Gupta and P. Thaddeus, *Astrophys. J.*, 2006, **652**, L141.

5 J. Cernicharo, M. Agúndez and M. Gúelin, *The Molecular Universe*, Cambridge University Press, Cambridge, 2011, p. 237.

6 M. Agúndez, J. Cernicharo, M. Guélin, C. Kahane, E. Roueff, J. Klos, F. J. Aoiz, F. Lique, N. Marcelino, J. R. Goicoechea, M. González García, C. A. Gottlieb, M. C. McCarthy and P. Thaddeus, *Astron. Astrophys.*, 2010, **517**, L2.

7 A. Remijan, H. Scolati, A. Burkhardt, P. Changala, S. Charnley, I. Cooke, M. Cordiner, H. Gupta, E. Herbst, K. Lee, R. Loomis, C. Shingledecker, M. Siebert, C. Xue, B. Mccarthy and M. C. McGuire, *Astrophys. J., Lett.*, 2023, **L45**, 944.

8 T. Ross, E. Baker, T. Snow, J. Destree, B. Rachford, M. Drosback and A. Jensen, *Astrophys. J.*, 2008, **684**, 358.

9 P. del Mazo-Sevillano, M. Lara, E. Yurtsever, M. Satta, R. Wester and F. Gianturco, *Astrophys. J.*, 2014, **973**, 17.

10 D. Field, *Astron. Astrophys.*, 2000, **362**, 774.

11 M. Jura, *Astrophys. J.*, 1975, **197**, 575.

12 M. A. Cordiner and T. J. Millar, *Astrophys. J.*, 2009, **697**, 68.

13 M. Satta, F. A. Gianturco, F. Carelli and R. Wester, *Astrophys. J.*, 2015, **799**, 228.

14 F. A. Gianturco, M. Satta, M. Mendolicchio, F. Palazzetti, A. Piserchia, V. Barone and R. Wester, *Astrophys. J.*, 2016, **830**, 2.

15 H. J. Werner and P. J. Knowles, *J. Chem. Phys.*, 1985, **82**, 5053.

16 P. J. Knowles and H. J. Werner, *Chem. Phys. Lett.*, 1985, **115**, 259.

17 K. R. Shamasundar, G. Knizia and H.-J. Werner, *J. Chem. Phys.*, 2011, **135**, 053101.

18 J. Cernicharo, J. Pardo, C. Cabezas, M. Agundez, B. Tercero, N. Marcelino, R. Fuentetaja, M. Guelin and P. de Vicente, *Astron. Astrophys.*, 2023, **670**, L19.

19 A. Faure, K. Szalewicz and L. Wiesenfeld, *J. Chem. Phys.*, 2011, **135**, 1229.

20 F. Khadri, A. Chefai and K. Hammami, *Mon. Not. R. Astron. Soc.*, 2020, **498**, 5159–5165.

21 E. Sahnoun, L. Wiesenfeld, K. Hammami and N. Jaidane, *J. Phys. Chem. A*, 2018, **122**, 3004–3012.

22 H. Massó and L. Wiesenfeld, *J. Chem. Phys.*, 2014, **141**, 365.

23 A. M. Arthurs and A. Dalgarno, *Proc. R. Soc. London, Ser. A*, 1960, **256**, 540.

21242 | *Phys. Chem. Chem. Phys.*, 2025, **27**, 21231–21243

This journal is © the Owner Societies 2025

24 D. Secrest, in *Atom – Molecule Collision Theory*, ed. R. B. Bernstein, Plenum, New York, 1979, p. 239.

25 D. Kouri and D. Hoffman, in *Multiparticle Quantum Scattering With Applications to Nuclear, Atomic and Molecular Physics*, ed. D. G. Truhlar and B. Simon, Springer, New York, NY, 1997, 89.

26 F. Gianturco, *The Transfer of Molecular Energies by Collisions: Recent Quantum Treatments*, Springer Verlag, Berlin, 1979.

27 J. Pardo, C. Cabezas, M. Agundez, B. Tercero, N. Marcelino, P. de Vicente, J. Guelin and M. Cernicharo, *Astron. Astrophys.*, 2023, **677**, A55.

28 R. Biswas, K. Giri, L. González-Sánchez, F. A. Gianturco, U. Louderaj, N. Sathyamurthy, A. Veselinova, E. Yurtsever and R. Wester, *Mon. Not. R. Astron. Soc.*, 2023, **522**, 5775–5787.

29 A. Fernandez-Ramos, J. A. Miller, S. J. Klippenstein and D. G. Truhlar, *Chem. Rev.*, 2006, **106**, 4518.

30 Y. Georgievskii and S. Klippenstein, *J. Chem. Phys.*, 2005, **122**, 194103.

31 J. M. Hutson and C. R. L. Sueur, *Comput. Phys. Commun.*, 2019, **241**, 9–18.

32 J. M. Hutson and C. R. L. Sueur, *MOLSCAT a program for non-reactive quantum scattering calculation on atomic and molecular collisions*, 2019, **https://github.com/molscat/molscat**.

33 O. Martinez, Z. Yang, N. Demarais, T. Snow and V. Bierbaum, *Astrophys. J.*, 2010, **720**, 173.

34 G. Mackay, L. D. Betowski, J. D. Payzant, H. Schiff and D. Bohme, *J. Phys. Chem.*, 1976, **80**, 2919–2922.

35 M. Khamesian, N. Douguet, S. Fonseca Dos Santos, O. Dulieu, M. Raoult and V. Kokoouline, *Eur. Phys. J. D*, 2016, **70**, 240–247.

36 K. Giri, L. González-Sánchez, F. A. Gianturco, U. Lourderaj, M. Santa Daría, S. Rana, N. Sathyamurthy, E. Yurtsever and R. Wester, *Mon. Not. R. Astron. Soc.*, 2024, **534**, 1950–1962.

37 K. M. Walker, F. Lique, F. Dumouchel and R. Dawes, *Mon. Not. R. Astron. Soc.*, 2017, **466**, 831–837.

This journal is © the Owner Societies 2025

Phys. Chem. Chem. Phys., 2025, **27**, 21231–21243 | **21243**